How to cite: Angew. Chem. Int. Ed. 2023, e202317526
doi.org/10.1002/anie.202317526

Catalysis

Consumer Grade Polyethylene Recycling via Hydrogenolysis on Ultrafine Supported Ruthenium Nanoparticles

*Shibashish D. Jaydev[+], Antonio J. Martín[+], Marc-Eduard Usteri, Katia Chikri, Henrik Eliasson, Rolf Erni, and Javier Pérez-Ramírez**

Abstract: Catalytic hydrogenolysis has the potential to convert high-density polyethylene (HDPE), which comprises about 30 % of plastic waste, into valuable alkanes. Most investigations have focused on increasing activity for lab grade HDPEs displaying low molecular weight, with limited mechanistic understanding of the product distribution. No efficient catalyst is available for consumer grades due to their lower reactivity. This study targets HDPE used in bottle caps, a waste form generated globally at a rate of approximately one million units per hour. Ultrafine ruthenium particles (1 nm) supported on titania (anatase) achieved up to 80 % conversion into light alkanes (C_1–C_{45}) under mild conditions (498 K, 20 bar H_2, 4 h) and were reused for three cycles. Small ruthenium nanoparticles were critical to achieving relevant conversions, as activity sharply decreased with particle size. Selectivity commonalities and peculiarities across HDPE grades were disclosed by a reaction modelling approach applied to products. Isomerization cedes to backbone scission as the reaction progresses. Within this trend, low molecular weight favor isomerization whilst high molecular weight favor cleavage. Commercial caps obeyed this trend with decreased activity, anticipating the influence of additives in realistic processing. This study demonstrates effective hydrogenolysis of consumer grade polyethylene and provides selectivity patterns for product control.

Introduction

High-density polyethylene (HDPE) is not only the most prevalent form of plastic waste (approximately 30 %), but also one of the most challenging chemical processes due to its non-hydrolyzable C–C backbone, high melting point, and high melting viscosity.[1] Pyrolysis, the only commercially available solution, offers limited control over product selectivity and suffers from high energy consumption,[2,3] imposing drawbacks that emerging strategies are trying to overcome.[4–7] Among them, catalytic hydrogenolysis is an increasingly favored approach[4,8–14] also applicable to other complex feedstocks such as biomass[15] due to its ability to selectively convert them into alkanes under mild conditions.

Unlike the rapidly growing literature covering the catalytic hydrogenolysis of polypropylene (PP) and low-density polyethylene (LDPE),[10,13,14,16] reports on HDPE are relatively scarce, with focus primarily on lab grade samples with weight average molecular weights below 100 kDa.[8,9,17–19] The low reactivity of HDPE generally leads to modest conversions, even with relatively low molecular weight feedstock, resulting, for example, in approximately 50 % solid residue after 6 h using m-SiO_2/Pt/SiO_2,[9] whereas small amounts of consumer grade HDPE have only been processed to a noticeable extent using hexane as a solvent on Ru/C (ca. 70 % conversion, 0.1 g HDPE, 1 h).[18] The low reactivity of HDPE compounds with the need to facilitate the catalyst-hydrogen-plastic contact to minimize mass transport limitations. Molecular dynamics simulations have pointed to the negligible diffusivity of H_2 in melted n-alkanes with long chains.[20] This forecasts that high performance may be connected with achieving effective agitation within the vessel despite the highly viscous nature of the melted plastic. Future engineering studies identifying optimal conditions may ensure more accurate and reproducible catalyst testing in this field.

In contrast to pyrolysis, where detailed models are available to largely rationalize reactivity patterns,[21] mechanistic descriptions for hydrogenolysis of lab- or commercial grade HDPE are still to be developed beyond pioneering computational simulations applied to describe adsorption energetics of model alkanes on specific surfaces such as Pt(111)[22] or monoclinic ZrO_2(−111).[17] Mechanistic tools more accessible to catalysis practitioners able to describe the main pathways favored by catalysts are thus highly desirable. It should also be noted that the prevalent use of lab grade

[*] S. D. Jaydev,[+] Dr. A. J. Martín,[+] M.-E. Usteri, K. Chikri, Prof. J. Pérez-Ramírez
Institute of Chemical and Bioengineering, Department of Chemistry and Applied Biosciences, ETH Zurich
Vladimir-Prelog-Weg 1, 8093 Zurich (Switzerland)
E-mail: jpr@chem.ethz.ch
H. Eliasson, Prof. R. Erni
Electron Microscopy Center, Swiss Federal Laboratories for Materials Science and Technology
Überlandstrasse 129, 8600 Dübendorf (Switzerland)
[+] These authors contributed equally to this work.

plastics for catalyst development is not limited to HDPE reports. For other polyolefins such as PP,[12,19] the extrapolation of results to more realistic or even similarly graded feedstocks has also proven to not be straightforward because of varying properties such as adsorption strength.[13,23,24] Recent simulations predict an acute decrease of the fraction of linear alkanes that are adsorbed on a metallic surface as the chain length increases and a direct correlation between the number of alkane-surface anchoring points and the branching degree.[22] These results suggest that polyolefins of different types may virtually be considered as different reactants and support a general *feedstock gap* in catalyst design studies on polyolefin hydrogenolysis hindering the development of efficient catalytic materials. A more targeted approach is thus necessary to meet the growing demand for enhanced chemical recycling of consumer grade HDPE.

This study focuses on the HDPE type employed in the production of soft drink bottle caps (melt flow index = 2.2; $M_w \approx 200$ kDa), which represents one of the most prevalent forms of plastic waste generated at a rate of around one million units per hour worldwide.[25] After observing the positive effect of smaller ruthenium nanoparticles supported on ceria to process LDPE,[26] reusable titania-supported ruthenium particles of ca. 1 nm are developed to achieve up to 80 % conversion into light alkanes (C_1–C_{45}) and the fundamental significance of small particle sizes disclosed. Beyond activity, the origin of the selectivity patterns and general trends could also be disclosed. The adaptation to HDPE of a reaction model we introduced for PP[14] allowing to close the C–C bond population balance gave access to quantification of isomerization, backbone scission, and demethylation contributions to the product pool. This pioneering analysis shows that the prevalent mechanistic route shifts from isomerization to backbone scission as the conversion degree increases. Expanding this investigation to plastic caps and other HDPE types between 100 and 6000 kDa verified this trend and showed how the degree of this shift, and to a more general extent the tendency to undergo cleavage, are determined by the plastic type. The slightly decreased conversion of plastic caps is discussed based on the reactivity of polyamides as common additives. Ultimately, this article describes successful processing of one of the most widespread kinds of plastic waste and provides reactivity patterns associated with its types.

Results and Discussion

Synthesis and Characterization of Titania-Supported Ultrafine Ruthenium Nanoparticles

The first step was to synthesize structured catalysts targeting 5 wt % ruthenium nanoparticles with variable size supported on titania. A simple impregnation procedure followed by different thermal treatments, described in detail in the Experimental Section of the Supporting Information, resulted in catalysts exhibiting different particle sizes used herein to label them with the code Ru*X*/TiO_2, where *X* represents the average particle size in nm. Figure 1a shows representative HAADF-STEM images of as-prepared catalysts (additional images are available in Figures S1–S2), from which a statistical analysis revealed average particle sizes of ca. 1 (Ru1/TiO_2), 4.5 (Ru5/TiO_2), and 17 nm (Ru17/TiO_2). EDX coupled to STEM confirmed the homogeneous distribution of ruthenium particles on the surface of titania (Figure 1b and Figure S1). Consistent with this, XRD analysis (Figure S3) displayed the expected pattern for the TiO_2 anatase carrier with no discernible signals attributable to ruthenium phases in the case of Ru1/TiO_2 and Ru5/TiO_2 due to their nanometric particle sizes. The larger particles in Ru17/TiO_2 manifested as reflections compatible with RuO_2 probably formed on exposure to air.

Catalytic Processing of Commercial Grade HDPE

Consumer grade HDPE used to produce soft carbonated drink caps with a melt flow index of 2.2 and a molecular weight $M_w = 200$ kDa (referred to in this article as $HDPE_{200}$, properties can be found in Table S1) was first processed using the catalysts described above according to the scheme depicted in Figure 2, for which a stepwise description can be found in the Experimental Section of the Supporting Information. Such a procedure made it possible to obtain the product distributions and the contributions of the main mechanistic pathways leading to them. The reference reaction conditions for catalyst evaluation ($T = 498$ K, $p_{H2} = 20$ bar, catalyst/plastic = 0.05, stirring rate = 750 rpm, $t = 4$ h) were chosen among the mildest in the literature of polyethylene hydrogenolysis[8–11,17,19,26] and taking into account our previous experience.[14] A photograph of the reactor inset and stirrer geometry as well as the preliminary evaluation of optimal stirring rates to alleviate mass transport effects have been presented in Figure S4 and S5. Product quantification was possible by combining (headspace) gas chromatography and proton nuclear magnetic resonance (^{1}H NMR) spectroscopy, providing the gas, liquid, and residue (defined as C_{45+}) fractions. These results served as input for the reaction modelling stage, which quantified the contributions of isomerization, backbone scission, and demethylation based on a C–C bond population balance facilitated by reaction modelling as explained in more detail in the following section.

Figure 3a presents the yields for the alkane fractions obtained after hydrogenolysis of $HDPE_{200}$ over Ru*X*/TiO_2. The highest total yield (76 %) corresponds to Ru1/TiO_2 followed by Ru5/TiO_2 and Ru17/TiO_2 showing an inverse linear correlation with the average particle size. Beyond the potential positive effect of enhanced ruthenium dispersion for decreasing particle sizes, temperature-programmed desorption experiments over Ru1/TiO_2 and Ru5/TiO_2 using heptane as a surrogate molecule for HDPE (Figure S4) suggest that electronic effects may have a critical role in rationalizing the better performance of small particles. Ru1/TiO_2 showed an overall milder adsorption strength with two identifiable desorption peaks, in contrast to the broad signal shifted toward higher temperatures obtained over Ru5/TiO_2.

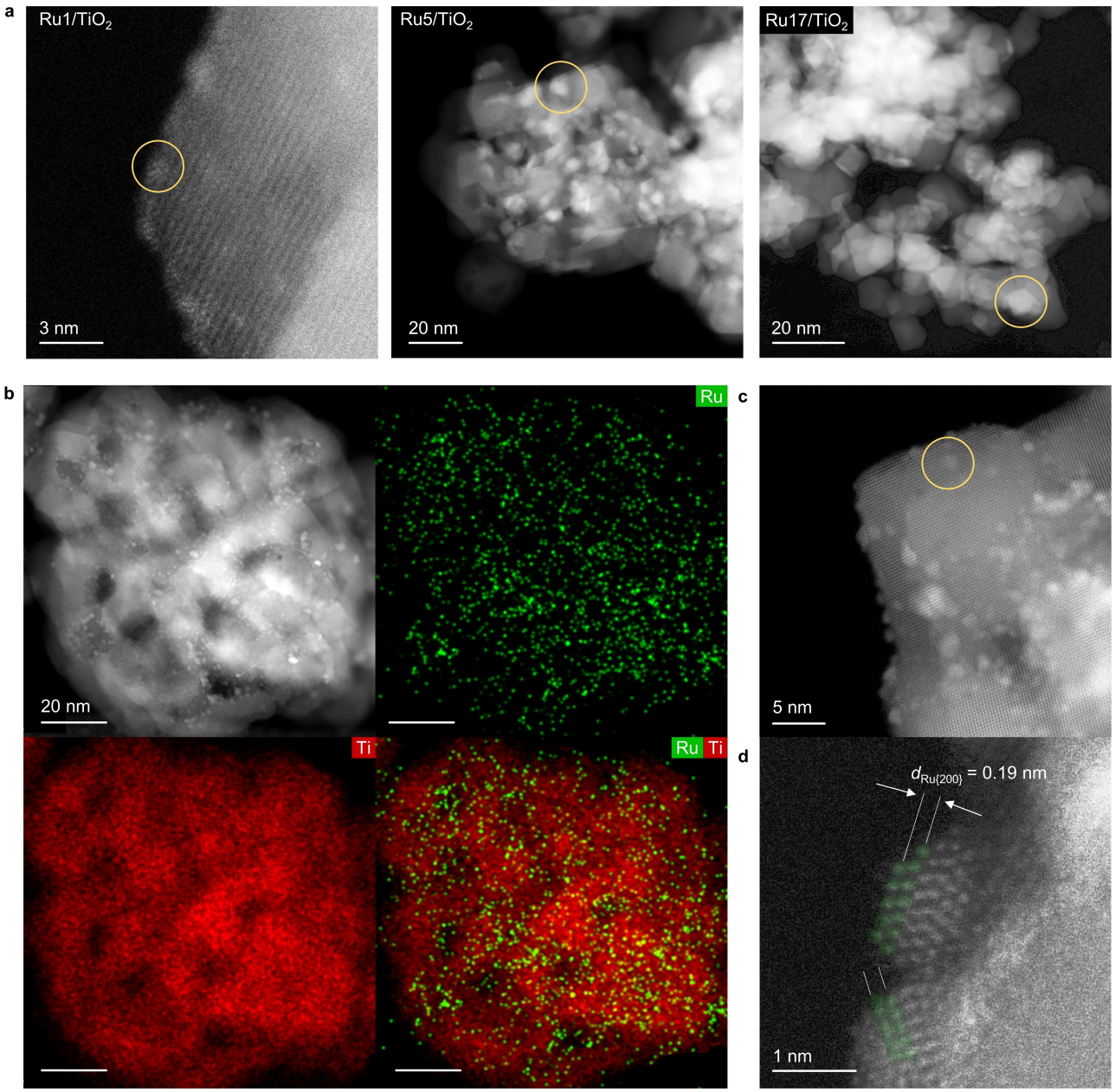

Figure 1. (a) STEM-HAADF images of as-prepared catalysts containing 5 wt% Ru with different average ruthenium particle sizes. Ru1/TiO_2: ~1 nm, Ru5/TiO_2: ~4.5 nm, Ru17/TiO_2: ~17 nm. For Ru1/TiO_2 after hydrogenolysis of $HDPE_{200}$, STEM-HAADF images (b) with corresponding EDX maps, (c) showing preserved ruthenium particle size, and (d) high magnification STEM image with identification of lattice plane. Color is added to atoms to guide the eye. Additional images are available in Figures S1, S2, and S7. Reaction conditions: $T = 498$ K, $p_{H2} = 20$ bar, catalyst/plastic = 0.05, stirring rate = 750 rpm, $t = 4$ h.

Weaker alkane-metal interactions may increase the exposure of longer polymer to the metal by freeing up the coordination sites more quickly after the reaction, which is aligned with the enhanced reactivity observed for small particles. Complementing this analysis with one of product distributions, a consistently larger fraction of C_1–C_5 (gas) and C_{21}–C_{44} (motor oil) over C_6–C_{20} (gasoline and diesel) products was a common feature of the results shown in Figure 2a. Similar bimodal product distributions have been previously observed for hydrogenolysis of laboratory grade HDPE on silica-supported platinum nanoparticles.[9] Computational analyses predicted that only alkanes in the C_{20}–C_{26} range tend to adsorb on a metallic surface through all their carbon atoms,[22] likely due to the enthalpy gains from full-length adsorption outweighing the entropic penalty associated with orientating the chain normal to the surface.[27] Upon full-length adsorption, the probability of forming any of the products becomes more uniform and cleavage into small molecules must rise compared to long chains. From this perspective, the most likely effect of

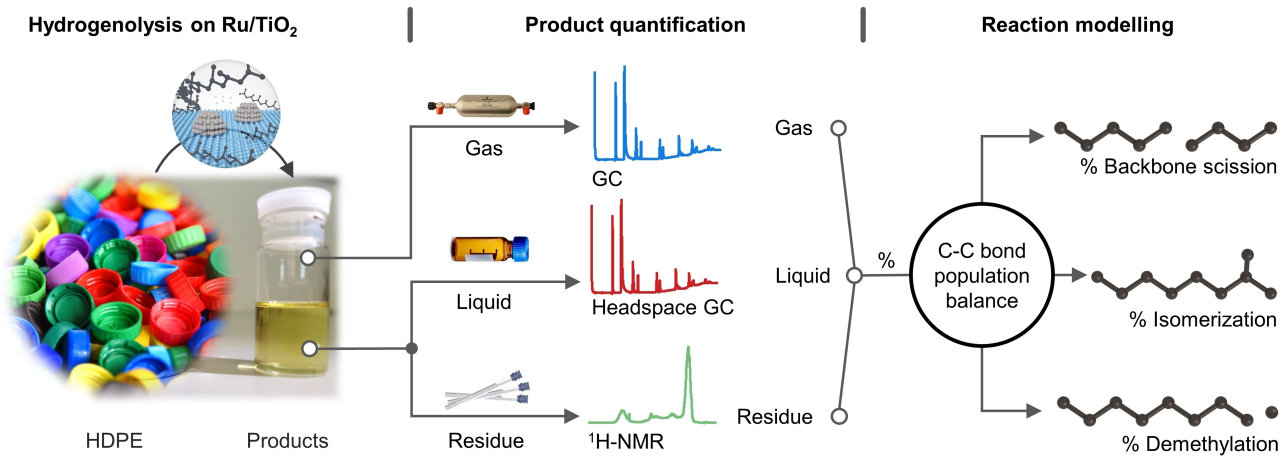

Figure 2. Workflow applied in this study, involving catalyst testing, product analysis, and reaction modelling. The mechanistic origin of observed selectivity patterns could be successfully traced upon determining contributions of main reaction pathways, which became accessible after interpreting product analysis through a C–C bond population balance.

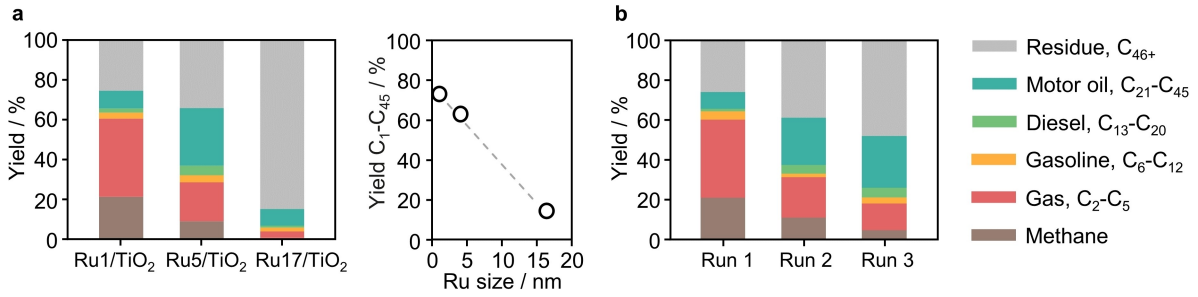

Figure 3. (a) Product yield after hydrogenolysis of $HDPE_{200}$ over the catalysts containing 5 wt% Ru and correlation between yield to C_1–C_{45} products and average Ru particle size. (b) Reusability test of $Ru1/TiO_2$ for hydrogenolysis of $HDPE_{200}$ over three consecutive runs. Numerical values are available in Table S2. Reaction conditions: $T = 498$ K, $p_{H_2} = 20$ bar, catalyst/plastic = 0.05, stirring rate = 750 rpm, $t = 4$ h

smaller particles appears to be increasing the activity, as the higher proportion of motor oil formed over $Ru5/TiO_2$ indicates an earlier cleavage stage compared to $Ru1/TiO_2$. Given the greatest potential shown by $Ru1/TiO_2$, it was subjected to three consecutive reactions (Figure 3b) to explore the reusability potential of these catalysts. Inspection of the figure shows that high conversions could be maintained through the cycles with an approximate 20% decrease in catalyst activity (Table S2), as suggested by the increasing yield of motor oil.

$Ru1/TiO_2$ exhibited excellent structural stability after the reaction, despite featuring sub-nanometric ruthenium particles. HAADF-STEM analysis disclosed that high dispersion, crystallinity, and particle size were retained, as shown in Figure 1c and Figure S7. Again, no reflection attributable to the ruthenium phase was present in the XRD analyses (Figure S3). These particles were predominantly metallic and crystalline in nature, as suggested by the measurement of the lattice plane spacings (Figure 1d). This behavior contrasts with the transition to a disordered and cationic state with distinct catalytic properties of sub-nanometric particles supported on ceria after reaction with LDPE,[26] recommending the development of deeper understanding of metal-support interactions in this reaction. In addition, further analysis by XPS concluded that the surface relation between metallic and oxidic ruthenium is approximately $Ru^0 : (Ru^{3+} + Ru^{4+}) = 1:1$ according to the deconvoluted signals (Figure S3). Besides the difficulty of assessing oxidic phases present under reaction conditions from ex situ analysis, this result reinforces the prevalence of the metallic phase under operation.

Having established the high activity and stability of $Ru1/TiO_2$ for the target $HDPE_{200}$, the next step was to investigate the extent to which this catalytic behavior could be extrapolated to other types, given the varying composition of real HDPE waste mixtures. Laboratory grade HDPE with one of the lowest commercially available molecular weights $M_w \sim 100$ kDa ($HDPE_{100}$, Table S1), commercial plastic caps based on $HDPE_{200}$ with the expected presence of dyes and additives (caps), and ultra-high molecular weight HDPE with the highest available molecular weight $M_w \sim 6000$ kDa ($HDPE_{6000}$, Table S1) were then investigated to represent the spectrum of potential feedstocks. Figure 4 contains the corresponding yields obtained using $Ru1/TiO_2$ under the same reaction conditions used previously. The processing of $HDPE_{100}$ and $HDPE_{200}$ under different reaction conditions over $Ru1/TiO_2$ (Figure S8 and S9) suggested a direct correlation between temperature and yield to

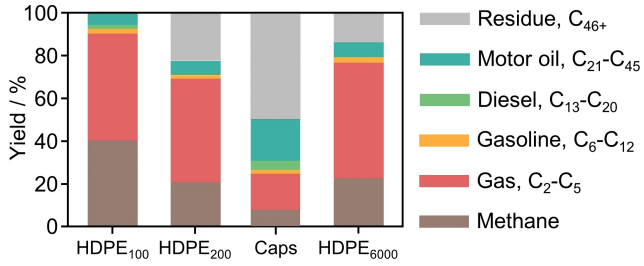

Figure 4. Product yield after hydrogenolysis over Ru1/TiO_2 of low ($HDPE_{100}$), medium ($HDPE_{200}$ and caps of carbonated drinks) and high ($HDPE_{6000}$) molecular weight HDPE. Numerical values are available in Table S2. Product distributions under other reaction conditions are available in Figures S8–S11. Reaction conditions: $T = 498$ K, $p_{H2} = 20$ bar, catalyst/plastic = 0.05, stirring rate = 750 rpm, $t = 4$ h.

C_1–C_{45} products. This can be ascribed to more favorable kinetics at higher temperatures and support a mild effect of mass transport limitations. With changing pressure, an optimum of 20 bar H_2 was found to maximize the yield to C_1–C_{45} products. This trend could be attributed to the competitive adsorption between hydrogen and the polyolefin fragments on the surface of Ru, which may prevent optimal rates of C–C bond activation at low and elevated pressures.[28] This effect has been reported for the hydrogenolysis of small alkanes on Ru, for which negative order in H_2 has also been claimed.[29,30]

Regarding product selectivity, all feedstocks showed the bimodal distribution of products seen in Figure 3a dominated by motor oil and/or gaseous alkanes (Table S2). This mechanistic feature thus appears to be independent of the HDPE feedstock. Gaseous products predominated for the cases of high C_1–C_{45} yields ($HDPE_{100}$, $HDPE_{200}$, $HDPE_{6000}$), whereas gaseous and motor oil did for the lower conversion case obtained from commercial caps. However, the trend observed for C_1–C_{45} yields cannot be easily rationalized on the base of different molecular weights. $HDPE_{100}$ exhibited the highest conversion (100 %) into C_1–C_{45} followed by $HDPE_{200}$, which was almost equaled by that of $HDPE_{6000}$. Notably, the conversion of the caps was significantly lower than that of its parent $HDPE_{200}$, clearly demonstrating the influence of additives present in real plastic waste and highlighting the need to consider realistic feedstocks in the design of catalysts for HDPE hydrogenolysis.

To rationalize the observed reactivity trend, we considered that similar chain length distributions in the products could have different mechanistic origins. The combination of pathways behind these product distributions could be successfully traced upon interpreting the set of products in the light of a C–C bond population balance described in the next section (reaction modelling stage in Figure 2) facilitated by the simple chemical structure of HDPE.

Quantification of Reaction Pathways

A previously reported model[14] for polypropylene hydrogenolysis based on product features obtained from GC and ^{1}H NMR analysis able to quantify the relative occurrence of backbone and demethylation was adapted to include isomerization (methyl shifts) to the case of HDPE. As new bonds are being formed at the expense of previously existing bonds, relative quantification of each type of carbon (primary, secondary, tertiary) present before and after the reaction allows for formulation of Equations (1)–(4) below as the total moles of carbon are conserved. This has been referred to as C–C bond population balance. The model, displayed considers the C–C bond balance of primary (p), secondary (s), and tertiary (t) carbon atoms in the reactant and products.

$$n_p = n_{p0} + 2\xi_{ss} \tag{1}$$

$$n_s = n_{s0} - 2\xi_{ss} - \xi_{ps} - \xi_{iso} \tag{2}$$

$$n_t = n_{t0} + \xi_{iso} \tag{3}$$

$$n_m = \xi_{ps} \tag{4}$$

Where n denotes the number of carbon atoms, and the suffix (p,s or t) denotes the type of carbon atom being referred to. For simplicity, the model assumes that n_{p0} (moles of primary carbons in the feedstock) and n_{t0} (moles of tertiary carbons in the feedstock) are negligible ($n_{p0} \ll n_{s0}$ and $n_{t0} \approx 0$ for HDPE). As secondary carbons make up almost the entirety of the starting feedstock, the model assumes that $n_{s0} \approx n_0$ (the total number of carbons present in the feedstock). The total number of carbons in the feedstock is obtained by dividing the total polyolefin feed by the molar mass of the -CH_2 group. The values in mmol of n_p, n_s and n_t were calculated from the integration of the ^{1}H NMR spectra regions corresponding to the carbon types (Figure 5a). These values change according to the type of the scission or isomerization as indicated by ξ_{ps} (primary-secondary scission), ξ_{ss}, (secondary-secondary scission), and ξ_{iso} (isomerization). Methane quantified using GC-FID (n_m) has been assumed to exclusively come from ξ_{ps} events, thus assuming the non-existence of a demethylation event following an isomerization (no primary-tertiary scissions). The resolution of the previous set of equations after incorporating the experimentally accessible parameters provided the value for ξ_{ps}, ξ_{ss}, and ξ_{iso}, enabling to compare their contributions to create the pool of products.

Prevalent Reaction Pathways for HDPE Types

Once this model was developed able to decipher the mechanistic origin of product distributions, the mapping of contributions from demethylation, backbone scission, and isomerization under a variety of operating conditions (p_{H2} = 10–30 bar, T = 448–498 K, Figures S8 to S10 and Table S3) for all HDPE feedstocks investigated followed. Some

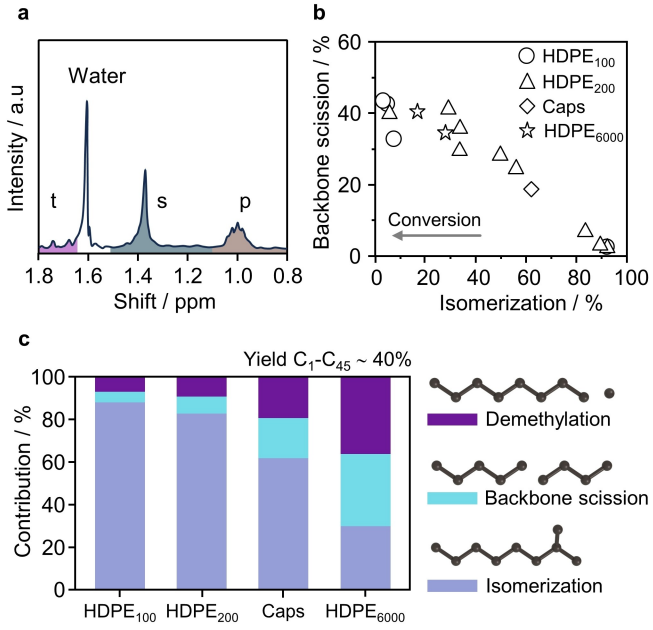

Figure 5. Product yield after hydrogenolysis over Ru1/TiO_2 of low ($HDPE_{100}$), medium ($HDPE_{200}$ and caps of carbonated drinks) and high ($HDPE_{6000}$) molecular weight HDPE. Numerical values are available in Table S2. Product distributions under other reaction conditions are available in Figures S8–S11. Reaction conditions: $T = 498$ K, $p_{H2} = 20$ bar, catalyst/plastic = 0.05, stirring rate = 750 rpm, $t = 4$ h.

general trends could thus be seen. For example, isomerization played a more prominent role at low conversion rates, as observed for $HDPE_{200}$ at different temperatures (Figure S8) or from the analysis of reusability experiments (Figure S9), for which isomerization becomes increasingly relevant with the number of cycles (from 8.4 to 48 %). In alignment, for the more reactive $HDPE_{100}$ isomerization played a negligible role (< 6 %) as shown in Figure S10, except for modest conversions forced by the lowest reaction temperature (448 K). The robustness of the model was successfully tested by comparing the predicted relevance of isomerization with the abundance of isomeric products detected by GC (Figure S12). The contributions of backbone scission were contained in a narrower range (20–40 %) and appeared to be positively related to the conversion.

All in all, these observations could be summarized in the tight inverse linear correlation displayed in Figure 5b between isomerization and backbone scission obeyed by all HDPE feedstock types. This relationship suggests a shift in the dominant pathway from isomerization to backbone scission as the conversion increases and points to a general mechanistic feature of HDPE hydrogenolysis over Ru/TiO_2 catalysts. This trend is, however, halted at high conversions since the degree of backbone scission tends to plateau due to the greater contribution of demethylation towards C–C cleavage as can be observed in Figure S13. This effect could be linked to observations developed over classical studies on hydrogenolysis claiming higher reactivity of longer chains to backbone scission due to increasing rotational entropy overcoming the large and almost constant activation enthalpies, which also leads to increasingly favored cleavage of non-terminal C–C bonds.[23,30] Similarly, increasing chain lengths favor isomerization yields in the presence of hydrogen.[31,32] Importantly, branching is predicted to increase the number of anchoring points between the polymer fragment and metallic surfaces, making it more susceptible to reaction.[22]

This finding was consistent with the similar product distribution obtained for $HDPE_{200}$ and $HDPE_{6000}$ in Figure 4. However, the distinct mechanistic behavior of all HDPE feedstock types, as shown in Figure 5c, only emerged after analysis of contributing pathways under similar degrees of conversion (yield C_1-C_{45} ~ 40 %, Table S2, colored symbols in Figure 5b). The degree to which the shift between isomerization and backbone scission occurs appears to correlate with the molecular weight, with lower molecular weight one being more prone to undergo isomerization, i.e., higher molecular weight being more prone to undergo cleavage events (backbone scission and demethylation). In particular, the comparison between $HDPE_{200}$ and $HDPE_{6000}$ shows strong differences, with isomerization largely dominating in the case of $HDPE_{200}$ and a more balanced contribution from the three pathways in the case of $HDPE_{6000}$.

In light of the same analysis, $HDPE_{200}$ and the caps shared the distribution of active pathways to a large extent. This result suggests that the main effect of the additives used in this HDPE application and for this class of catalysts is to reduce their activity (Figure 4) without noticeable mechanistic effects. Terminal amides with unsaturated backbones such as stearamide ($C_{18}H_{37}NO$) or behenamide ($C_{22}H_{45}NO$) are ubiquitously used as slip agents in the manufacturing of plastic caps in concentrations ranging from 500 to 1500 ppm.[33] Recent investigations have revealed the high activity of ruthenium nanoparticles supported on ceria to transform polyamides into methane, water, and ammonia, with C–O and C–N bonds being preferentially cleaved.[34] This result strongly indicates the presence of ammonia and water in the reaction mixture at early reaction stages, which may interact with the ruthenium surface reducing its ability to develop C–C cleaving, for example, by either blocking it in the case of ammonia being decomposed[35] or by triggering surface reconstruction in the case of water adsorption.[36]

Despite the unavailability of the precise composition of the plastic caps, this reasoning was first confirmed by the presence of ca. 0.5 wt % nitrogen in the caps together with chlorine in the ppm range (likely present in pigments), as revealed by X-ray fluoresce and hinting at two potential origins of catalyst deactivation. Chlorine is a well-known poison in pyrolysis of plastic waste,[4] so we focused on the unexplored role of nitrogen. As expected, behenamide was readily transformed by Ru1/TiO_2 into a gas mixture (Figure S14, Table S2). The same figure shows that the addition of water to the mixture of Ru1/TiO_2 and $HDPE_{200}$ did not significantly alter the catalyst activity, but the addition of 400 ppm of ammonia (mimicking the expected range from full conversion of plastic caps), led to a significantly lower conversion, suggesting that ammonia stemmed from nitrogen-containing additives could poison catalyst activity.

These aspects highlight the importance of additives in future catalyst design efforts.

Conclusion

Ruthenium nanoparticles of approximately 1 nm supported on titania operate as the first highly effective catalyst for the hydrogenolysis of commercial grade polyethylene used to make plastic caps, with small particle size being critical to achieving relevant activity rates. General selectivity patterns could also be disclosed and rationalized based on reaction modelling able to quantify the contributions of isomerization, backbone scission, and demethylation for the full range of commercially available HDPE types and bottle caps. A tight and universal trade-off between isomerization and backbone scission dependent on the conversion degree emerged, disclosing a general feature of HDPE reactivity over this family of catalysts. However, particularities within this general feature were also observed, since isomerization is more prevalent in lower molecular weight HDPE and backbone scission in higher molecular weight ones. The presence of additives in commercial caps resulted in reduced activity compared to its virgin counterpart without noticeable mechanistic changes, likely due to the ubiquitous use of highly reactive amides as slip agents leading to the presence of ammonia in the reaction mixture. Overall, these results present the first highly active catalyst for the hydrogenolysis of one of the most prevalent and challenging forms of plastic waste, underline the commonalities and differences in reactivity across different HDPE types, and provide accessible understanding tools for selectivity patterns.

Experimental Section

Detailed experimental and computational procedures can be found in the Supporting Information.

Supporting Information

Supporting Information is available from the Wiley Online Library or the author. Data presented in the main figures of the manuscript are publicly available through the Zenodo repository (https://doi.org/10.5281/zenodo.10137897). Other source data are available from the corresponding author upon request.

Author Contributions

S.D.J. conceptualized and performed the experiments and analyzed the data. A.J.M conceptualized the experiments, analyzed the data, and supervised the study. S.D.J. and M.-E.U. developed the mathematical model. K.C. and H.E. performed the experiments and analyzed the data, R.E. conceptualized the experiments and supervised the study, J.P.-R. conceptualized the experiments, conceived, and supervised the entire study. All the authors were involved in the development of the manuscript.

Acknowledgements

This work was supported by ETH Zurich through an ETH Research Grant (ETH-40 20-2). Dr. Thaylan P. Araújo and Vera Giulimondi are thanked for XPS characterization.

Conflict of Interest

The authors declare no conflict of interest.

Data Availability Statement

The data that support the findings of this study are openly available in Zenodo at https://doi.org/10.5281/zenodo.10137897, reference number 10137897.

Keywords: Chemical Plastic Recycling · Heterogenous Catalysis · Polyethylene Hydrogenolysis · Ruthenium Nanoparticles · Selectivity

[1] S. Kumar, A. K. Panda, R. K. Singh, *Resour. Conserv. Recycl.* **2011**, *55*, 893–910.
[2] S. D. Anuar Sharuddin, F. Abnisa, W. M. A. W. Daud, M. K. Aroua, *Energy Convers. Manage.* **2016**, *115*, 308–326.
[3] M. I. Jahirul, M. G. Rasul, D. Schaller, M. M. K. Khan, M. M. Hasan, M. A. Hazrat, *Energy Convers. Manage.* **2022**, *258*, 115451.
[4] A. J. Martín, C. Mondelli, S. D. Jaydev, J. Pérez-Ramírez, *Chem* **2021**, *7*, 1487–1533.
[5] J. N. Hancock, J. E. Rorrer, *Appl. Catal. B* **2023**, *338*, 123071.
[6] I. Vollmer, M. J. F. Jenks, M. C. P. Roelands, R. J. White, T. van Harmelen, P. de Wild, G. P. van der Laan, F. Meirer, J. T. F. Keurentjes, B. M. Weckhuysen, *Angew. Chem. Int. Ed.* **2020**, *59*, 15402–15423.
[7] C. Zhang, Q. Kang, M. Chu, L. He, J. Chen, *Trends Chem.* **2022**, *4*, 822–834.
[8] G. Celik, R. M. Kennedy, R. A. Hackler, M. Ferrandon, A. Tennakoon, S. Patnaik, A. M. Lapointe, S. C. Ammal, A. Heyden, F. A. Perras, M. Pruski, S. L. Scott, K. R. Poeppelmeier, A. D. Sadow, M. Delferro, *ACS Cent. Sci.* **2019**, *5*, 1795–1803.
[9] A. Tennakoon, X. Wu, A. L. Paterson, S. Patnaik, Y. Pei, A. M. LaPointe, S. C. Ammal, R. A. Hackler, A. Heyden, I. I. Slowing, G. W. Coates, M. Delferro, B. Peters, W. Huang, A. D. Sadow, F. A. Perras, *Nat. Catal.* **2020**, *3*, 893–901.
[10] Y. Nakaji, M. Tamura, S. Miyaoka, S. Kumagai, M. Tanji, Y. Nakagawa, T. Yoshioka, K. Tomishige, *Appl. Catal. B* **2021**, *285*, 119805.
[11] J. E. Rorrer, G. T. Beckham, Y. Román-Leshkov, *JACS Au* **2021**, *1*, 8–12.
[12] P. A. Kots, S. Liu, B. C. Vance, C. Wang, J. D. Sheehan, D. G. Vlachos, *ACS Catal.* **2021**, *11*, 8104–8115.
[13] S. D. Jaydev, A. J. Martín, J. Pérez-Ramírez, *ChemSusChem* **2021**, *14*, 5179–5185.
[14] S. D. Jaydev, M. E. Usteri, A. J. Martín, J. Pérez-Ramírez, *Chem Catal.* **2023**, *3*, 100564.

[15] P. Mäki-Arvela, M. Martínez-Klimov, D. Y. Murzin, *Fuel* **2021**, *306*, 121673.
[16] Q. Kang, M. Chu, P. Xu, X. Wang, S. Wang, M. Cao, O. Ivasenko, T.-K. Sham, Q. Zhang, Q. Sun, J. Chen, *Angew. Chem. Int. Ed.* **2023**, *62*, e202313174.
[17] S. Chen, A. Tennakoon, K. E. You, A. L. Paterson, R. Yappert, S. Alayoglu, L. Fang, X. Wu, T. Y. Zhao, M. P. Lapak, M. Saravanan, R. A. Hackler, Y. Y. Wang, L. Qi, M. Delferro, T. Li, B. Lee, B. Peters, K. R. Poeppelmeier, S. C. Ammal, C. R. Bowers, F. A. Perras, A. Heyden, A. D. Sadow, W. Huang, *Nat. Catal.* **2023**, *6*, 161–173.
[18] C. Jia, S. Xie, W. Zhang, N. N. Intan, J. Sampath, J. Pfaendtner, H. Lin, *Chem Catal.* **2021**, *1*, 437–455.
[19] J. E. Rorrer, C. Troyano-Valls, G. T. Beckham, Y. Román-Leshkov, *ACS Sustainable Chem. Eng.* **2021**, *9*, 11661–11666.
[20] Z. A. Makrodimitri, D. J. M. Unruh, I. G. Economou, *Phys. Chem. Chem. Phys.* **2012**, *14*, 4133–4141.
[21] S. E. Levine, L. J. Broadbelt, *Polym. Degrad. Stab.* **2009**, *94*, 810–822.
[22] M. Zare, P. A. Kots, S. Caratzoulas, D. G. Vlachos, *Chem. Sci.* **2023**, *14*, 1966–1977.
[23] D. D. Hibbitts, D. W. Flaherty, E. Iglesia, *J. Phys. Chem. C* **2016**, *120*, 8125–8138.
[24] A. M. Goda, M. Neurock, M. A. Barteau, J. G. Chen, *Surf. Sci.* **2008**, *602*, 2513–2523.
[25] Statista.com, "Production of polyethylene terephthalate bottles worldwide from 2004 to 2021," can be found under https://www.statista.com/statistics/723191/production-of-polyethylene-terephthalate-bottles-worldwide/, **2021**.
[26] L. Chen, L. C. Meyer, L. Kovarik, D. Meira, X. I. Pereira-Hernandez, H. Shi, K. Khivantsev, O. Y. Gutiérrez, J. Szanyi, *ACS Catal.* **2022**, *12*, 4618–4627.
[27] K. C. Daoulas, V. A. Harmandaris, V. G. Mavrantzas, *Macromolecules* **2005**, *38*, 5780–5795.
[28] L. Chen, Y. Zhu, L. C. Meyer, L. V. Hale, T. T. Le, A. Karkamkar, J. A. Lercher, O. Y. Gutiérrez, J. Szanyi, *React. Chem. Eng.* **2022**, *7*, 844–854.
[29] J. H. Sinfelt, *Catal. Rev.* **1970**, *3*, 175–205.
[30] D. W. Flaherty, E. Iglesia, *J. Am. Chem. Soc.* **2013**, *135*, 18586–18599.
[31] P. Mäki-Arvela, T. A. K. Khel, M. Azkaar, S. Engblom, D. Y. Murzin, *Catalysts* **2018**, *8*, 534.
[32] L. C. Gomes, D. de Oliveira Rosas, R. C. Chistone, F. M. Z. Zotin, L. R. R. de Araujo, J. L. Zotin, *Fuel* **2017**, *209*, 521–528.
[33] M. Gall, A. Schweighuber, W. Buchberger, R. W. Lang, *Sustainability* **2020**, *12*, 10378.
[34] X. Wu, W.-T. Lee, R. C. Turnell-Ritson, P. C. L. Delannoi, K.-H. Lin, P. J. Dyson, *Nat. Commun.* **2023**, *14*, 6524.
[35] W. Tsai, W. H. Weinberg, *J. Phys. Chem.* **1987**, *91*, 5302–5307.
[36] S. Maier, P. Cabrera-Sanfelix, I. Stass, D. Sánchez-Portal, A. Arnau, M. Salmeron, *Phys. Rev. B* **2010**, *82*, 75421.

Manuscript received: November 17, 2023
Accepted manuscript online: December 17, 2023
Version of record online: ■■, ■■

Research Articles

Catalysis

S. D. Jaydev, A. J. Martín, M.-E. Usteri, K. Chikri, H. Eliasson, R. Erni, J. Pérez-Ramírez* **e202317526**

Consumer Grade Polyethylene Recycling via Hydrogenolysis on Ultrafine Supported Ruthenium Nanoparticles

Ruthenium particles of ~1 nm supported on titania achieved via hydrogenolysis up to 80% conversion of HDPE used in bottle caps into light alkanes at mild conditions and showed reusability. General selectivity trends were disclosed across HDPE types. Isomerization cedes to backbone scission as reaction progresses, nuanced by HDPE type.